

Access to this work was provided by the University of Maryland, Baltimore County (UMBC) ScholarWorks@UMBC digital repository on the Maryland Shared Open Access (MD-SOAR) platform.

Please provide feedback Please support the ScholarWorks@UMBC repository by emailing scholarworks-group@umbc.edu and telling us what having access to this work means to you and why it's important to you. Thank you.

Computational Study on the Effects of Unsteady Freestream on an Airfoil Performance at Low Reynolds Numbers

Naresh Poudel¹ and Meilin Yu²

University of Maryland, Baltimore County, Baltimore, MD, 21250, USA

and

John T Hrynuk³

Combat Capabilities Development Command - Army Research Lab, Aberdeen Proving Ground, MD, 21005, USA

Computational studies of the response of a NACA0012 airfoil at varying angles of attack (α) to freestream turbulence at low Reynolds numbers (i.e., 12,000 based on the airfoil chord length) are conducted in this work. The unsteady freestream is generated by placing an array of circular cylinders upstream of the airfoil. The presence of moderate freestream turbulence (~5%) affected the formation of laminar separation bubbles near the leading edge of the airfoil, which has significant impacts on the aerodynamic performance. The study was able to recreate the maximum lift coefficient of the airfoil in unsteady freestream turbulence observed in experiments, which is higher than that for the airfoil in a uniform freestream. In general, the present numerical results agree reasonably well with those from experimental studies. This work also demonstrates that three-dimensional (3D) simulations with high-order accurate numerical methods predict the lift coefficient more accurately than lower dimension (i.e., 2D) or lower order 3D methods.

I. Nomenclature

Re	= Reynolds Number
c	= Chord
t	= Time
Δt	= Time step
t^*	= Convective time
U_∞	= Freestream velocity
TG	= Turbulence Generator
α	= Angle of Attack
C_L	= Lift coefficient
MAV	= Micro Air Vehicles
UAV	= Unmanned Aerial Vehicles
LBS	= Laminar Separation Bubble

¹ Graduate Student, Department of Mechanical Engineering, and AIAA Student Member. Email: npoudel1@umbc.edu.

² Associate Professor, Department of Mechanical Engineering, and AIAA Senior Member. Email: mlyu@umbc.edu.

³ Mechanical Research Engineer, Vehicle Technology Directorate, CCDC Army Research Lab.

II. Introduction

Studying aerodynamics at low Reynolds (Re) numbers has attracted extensive attention of researchers with the hope to better design Micro Air Vehicles (MAVs), small unmanned aerial vehicles (UAVs) and small scale wind turbines [1]. Most MAVs operate within the atmospheric boundary layer where a high level of freestream turbulence is present. Unfortunately, the high relative freestream turbulence can cause flight instability [2]. Under turbulent conditions, the time-averaged lift coefficient of a thin flat-plate airfoil has been shown to increase linearly with angles of attack (α) for $\alpha < 10^\circ$, which is consistent with the prediction of the classical thin-airfoil theory. When α exceeds 10° , an early stall is observed [3]. It has also been observed that boundary layers on thicker airfoil surfaces at low Reynolds numbers are sensitive to freestream turbulence and boundary layer turbulators like surface roughness [4–6]. Experimental studies have shown that at lower Reynolds numbers it is typical for Laminar Separation Bubbles (LSBs) to develop on the suction side of airfoil. The size and position of those LSBs are often diminished and delayed when freestream turbulence and turbulators are present [5]. The effects of freestream turbulence on airfoil performance at low Reynolds numbers ($Re < 10^5$) are still not well understood and have complex underlying flow physics. This study will investigate the fundamental flow physics underlying the boundary layer development of a static airfoil in the presence of freestream turbulence and characterize the corresponding aerodynamic performance.

The influence of freestream turbulence on airfoil performance has attracted considerable interest. Hoffmann [7] performed an experimental study on a NACA0015 airfoil at Reynolds number 2.5×10^5 , varying the turbulence intensities from 0.25% to 9.0%. Their results showed freestream turbulence increased the maximum lift coefficient by up to 30%. Laitone [8] measured the lift and drag for Reynolds number less than 70,000 on a NACA0012 airfoil, a thin flat plate and a cambered plate. The NACA0012 airfoil was observed to be particularly sensitive to Reynolds number variations or upstream turbulence level at low Reynolds number when flat and chamber plates. Mish and Devenport [9] and Gilling et al. [10] also showed that an increase in turbulence intensity can enhance the lift for a NACA0015 airfoil at much higher Reynolds numbers, $1.17 - 1.5 \times 10^6$. Huang and Lee [11] studied the freestream turbulence effects on the aerodynamics characteristics of a NACA0012 airfoil at Reynolds number $0.5 - 1.5 \times 10^5$ with varying turbulence intensities from 0.2% to 0.65%. Their study showed that the influence of freestream turbulence is significant when the turbulence intensity is smaller than 0.45%. Under this condition the lift coefficient increases with the increase in turbulence intensity delaying stall. Wang et al. [12] found that the freestream turbulence has more influence on the shear layer separation, reattachment, transition, and formation of the separation bubble at low Reynolds numbers compared to that at higher ones. Conger and Ramaprian [13] experimentally investigated the NACA0015 airfoil pitching upward in a water channel with relatively higher freestream turbulence level (0.8-1.0%). They reported a larger magnitude of pressure and aerodynamic forces in their study than the previous measurements obtained at similar Reynolds numbers and pitch rates, suggesting that turbulence effects may extend static measurements.

Laminar separation bubbles are an important flow feature for airfoils at low Reynolds numbers and can often determine the performance of the airfoil. An increase in freestream turbulence can shorten the length of, or sometimes eliminate, the laminar separation bubble [14]. Sicot et al. [15] showed that the oscillation length of the point of separation increases when the flow separation point moves towards the leading edge. The increase in stall angle and maximum lift coefficient ($C_{L_{max}}$) are found to be caused by eddies of different scales in freestream turbulence [16]. The stall angle is always larger for flows with small scale turbulence than for larger turbulent scales.

Flows with small-scale free stream turbulence also had a smoother and more controllable behavior in the near-stall region. Studies done by Cruz [14], Tsuchiya et al. [17], Ravi et al. [18] and Delnero et al. [16] showed that the stall angle is increased with increased freestream turbulence. The studies conducted by Cruz [14] and Ravi et al. [18] also showed that the increase in freestream turbulence levels results in an increase in C_{Lmax} , but this wasn't observed in all studies and appears to be dependent on the airfoil and Reynolds number.

Coder and Maughmer [19] observed that theoretical methods tend to over-predict the maximum lift coefficient when compared with experimental results for airfoils at low Reynolds numbers. High-order computational fluid dynamics (CFD) methods had been proven more accurate and efficient than the conventional methods to capture the complex flow structures [20,21].

The goal of the current study is to characterize the aerodynamic performance of a NACA0012 airfoil under unsteady freestream conditions. This study will also evaluate the turbulence generation method and model fidelity needed to match experimentally observed results. Simulated freestream turbulence will be numerically generated and the airfoil will be placed a variety of angles of attack at low Reynolds number ($Re = 12,000$). A variety of high order numerical simulations will be compared to determine the model fidelity required to accurately predict airfoil performance in turbulent conditions. The results from these simulations are also compared with experimental results.

III. Numerical Methods

Governing Equations

Unsteady compressible Navier-Stokes equations in conservation form are considered in the physical domain (t, x, y, z) as follows:

$$\frac{\partial Q}{\partial t} + \frac{\partial F}{\partial x} + \frac{\partial G}{\partial y} + \frac{\partial H}{\partial z} = 0, \quad (1)$$

where $Q = (\rho, \rho u, \rho v, \rho w, E)^T$ are conservative variables, ρ is the density of fluid, u, v and w are the x-, y- and z-components of the velocity and E is the total energy given by $E = \frac{p}{\gamma-1} + \frac{1}{2}\rho(u^2 + v^2 + w^2)$ for a perfect gas, in which p is the pressure and γ is the constant specific heat capacity ratio. The total energy formula is used to close the solution. The flux vectors (F, G and H) are total flux vectors which the inviscid and viscous flux terms in the x-, y- and z-direction, respectively. To facilitate numerical simulation, the governing equation (1) in the physical domain (t, x, y, z) is transformed into a computational domain (τ, ξ, η, ζ) as defined by Eq. (2). In the coordinate transformation, $\tau = t$ and $(\xi, \eta, \zeta) \in [-1, 1] \times [-1, 1] \times [-1, 1]$, which is defined by a standard unit element in the computational domain.

$$\frac{\partial \tilde{Q}}{\partial \tau} + \frac{\partial \tilde{F}}{\partial \xi} + \frac{\partial \tilde{G}}{\partial \eta} + \frac{\partial \tilde{H}}{\partial \zeta} = 0, \quad (2)$$

where

$$\begin{cases} \tilde{Q} = |J|Q \\ \tilde{F} = |J|(Q\xi_\tau + F\xi_x + G\xi_y + H\xi_z) \\ \tilde{G} = |J|(Q\eta_\tau + F\eta_x + G\eta_y + H\eta_z) \\ \tilde{H} = |J|(Q\zeta_\tau + F\zeta_x + G\zeta_y + H\zeta_z) \end{cases} \quad (3)$$

For this coordinate transformation, the Jacobian matrix is written in the following form:

$$J = \frac{\partial(x, y, z, t)}{\partial(\xi, \eta, \zeta, \tau)} = \begin{pmatrix} x_\xi & x_\eta & x_\zeta & x_\tau \\ y_\xi & y_\eta & y_\zeta & y_\tau \\ z_\xi & z_\eta & z_\zeta & z_\tau \\ 0 & 0 & 0 & 1 \end{pmatrix}. \quad (4)$$

The inverse transformation must also exist for a non-singular transformation, which can be related to the Jacobian matrix as:

$$J^{-1} = \frac{\partial(\xi, \eta, \zeta, \tau)}{\partial(x, y, z, t)} = \begin{pmatrix} \xi_x & \xi_y & \xi_z & \xi_t \\ \eta_x & \eta_y & \eta_z & \eta_t \\ \zeta_x & \zeta_y & \zeta_z & \zeta_t \\ 0 & 0 & 0 & 1 \end{pmatrix}. \quad (5)$$

Spatial Discretization and Time Integration Methods

The Flux Reconstruction/Correction Procedure via Reconstruction (FR/CPR) [20–26] method is used to solve the governing equations. A brief introduction of the FR/CPR method is discussed in this section for the sake of completeness, but a full discussion of the method can be found in [20]. When using the FR/CPR method, the flux terms in Eq. (2) have two parts: local fluxes constructed from local solutions and correction fluxes constructed on the element interfaces. These correction fluxes consider the differences between the local fluxes and the common fluxes. This can be expressed as:

$$\begin{cases} \tilde{F}(\xi, \eta, \zeta) = \tilde{F}^{loc}(\xi, \eta, \zeta) + \tilde{F}^{cor}(\xi, \eta, \zeta) \\ \tilde{G}(\xi, \eta, \zeta) = \tilde{G}^{loc}(\xi, \eta, \zeta) + \tilde{G}^{cor}(\xi, \eta, \zeta) \\ \tilde{H}(\xi, \eta, \zeta) = \tilde{H}^{loc}(\xi, \eta, \zeta) + \tilde{H}^{cor}(\xi, \eta, \zeta) \end{cases} \quad (6)$$

When substituting Eq. (6) into Eq. (2), the governing equations can be reformulated as:

$$\frac{\partial \tilde{Q}}{\partial \tau} + \left(\frac{\partial \tilde{F}^{loc}}{\partial \xi} + \frac{\partial \tilde{G}^{loc}}{\partial \eta} + \frac{\partial \tilde{H}^{loc}}{\partial \zeta} \right) + \left(\frac{\partial \tilde{F}^{cor}}{\partial \xi} + \frac{\partial \tilde{G}^{cor}}{\partial \eta} + \frac{\partial \tilde{H}^{cor}}{\partial \zeta} \right) = 0, \quad (7)$$

In this study, the inviscid common fluxes at the cell interfaces are calculated using a Roe approximate Riemann Solver [27] and the common viscous fluxes at the cell interfaces were obtained by the approach developed by Bassi and Rebay [28]. The method-of-line approach was used to conduct time-marching. In this approach, Equation (1) can be written as

$$\frac{\partial Q}{\partial t} = R(Q), \quad (8)$$

The explicit first stage, singly diagonally implicit Runge-Kutta (ESDIRK) method [25,26] was used for time integration, which is written as

$$\begin{cases} Q^{n+1} = Q^n + \Delta t \sum_{i=1}^s b_i R(Q_i) \\ Q_i = Q^n + \Delta t \sum_{j=1}^i a_{ij} R(Q_j), \quad i = 1, \dots, s, \end{cases} \quad (9)$$

where s is the number of stages and

$$a_{ii} = \begin{cases} 0, & i = 1, \\ \omega, & i \neq 1. \end{cases} \quad (10)$$

Equation (9) can then be written as

$$\begin{cases} Q^{n+1} = Q^n + \Delta t \sum_{i=1}^s b_i R(Q_i), \\ Q_1 = Q^n, \\ Q_i = \Delta t \omega R(Q_i) + Q^n + \Delta t \sum_{j=1}^{i-1} a_{ij} R(Q_j), \quad i = 2, \dots, s, \end{cases} \quad (11)$$

In this study, the second-order, three-stage ESDIRK2 and forth-order, sixth-stage ESDIRK4 with the time step of 10^{-2} were used.

Computational Domain

Figure 1 shows the schematic of 2D computational domain used for the numerical study. The dimensions of the computational domain are loosely based on the wind tunnel test section of the experiment at the U.S. Army Research Lab (ARL). For these simulations a fixed inlet and outlet boundary were used. For the 2D simulations symmetry boundary conditions were used for the top and bottom. An array of cylinders was placed perpendicular to a uniform freestream to generate turbulence in a similar manner to the Medium Turbulence Generator (MTG) experiment. This is a simplified version of the grid turbulence used in separate experiment, which used a grid of cylinders. The ratio of distance between cylinders (L) to the cylinder diameter (d), i.e. L/d is 3. For the 3D simulation, the 2D grid was extruded to a distance $s/c = \pi d$ in the spanwise direction. The Reynolds number based on diameter of cylinder is around 1900 and the spanwise length equal to πd is sufficient to capture 3D effects [29]. The periodic boundary conditions on the top, bottom and spanwise direction were used in the 3D simulations.

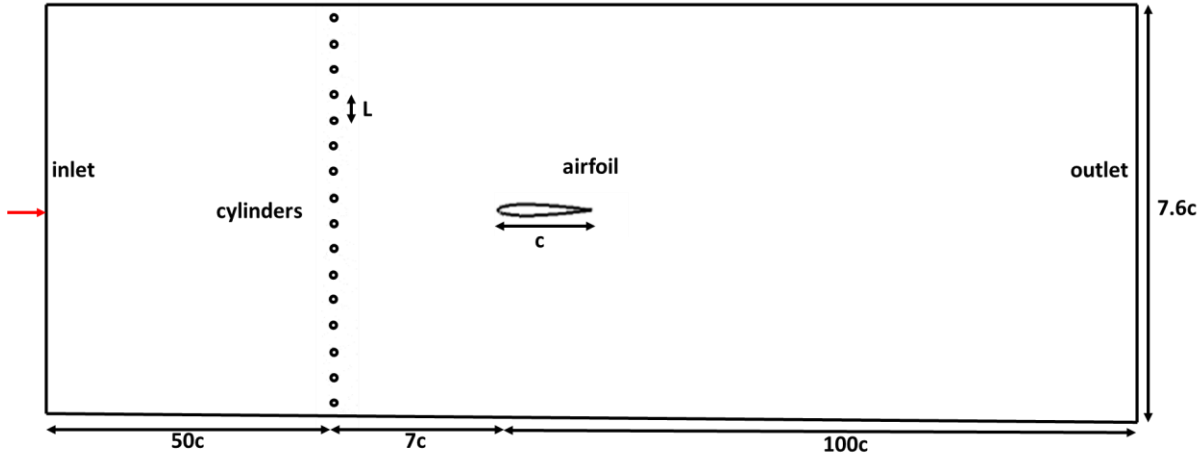


Figure 1: An illustration of the computational domain.

IV. Results and Discussions

The flow field downstream of the cylinder array was characterized without the wing to evaluate the turbulence generated. The vortices produced by the cylinders interact and mix with each other and, after a certain distance, a more homogenous field of turbulence is developed as shown in Figure 2 (a) and (b). In the 2D simulation, shown in Figure 2 (a), large scale vortices were observed near the future wing location whereas in 3D simulation the vortices broke down into small eddies (see Figure 2(b)). A numerical probe, equivalent to a hot-wire probe in experiments, was placed in the computational domain at the location where the wing was planned to be placed in later studies. The velocity power spectrum for 2D and 3D simulations were compared in Figure 2(c). The power spectral density (PSD) of the velocity for 2D and 3D simulations show that the energy decay region of -3 and $-5/3$ respectively. The turbulence intensity at the probe location for 2D simulation was also found to be around 7 times larger than in the 3D simulation. The higher turbulence intensity in 2D simulation was due to larger vortex structures that could not break down as rapidly as they could in the 3D simulation. Figure 2 (d) shows the velocity power spectrum for 3D simulation compared with an experimental result obtained at ARL in the wind tunnel. The turbulence intensity is for this case was around 5%, closely matching the experimental value of 4.8%. The power spectral density (PSD) analysis of the velocity shows the region of $-5/3$ energy decay for both computation and experiment, Figure 2 (d). The 2D and 3D characterization of the turbulence generator showed that the 3D simulation results closely matched with the experimental results. The results also showed that the 2D simulation produced a highly unsteady flow, but not one that reflects real-world turbulence. However, the results suggest that similar levels of unsteadiness could be reached by allowing the flow to develop over a much longer distance, but that was not investigated as part of this study.

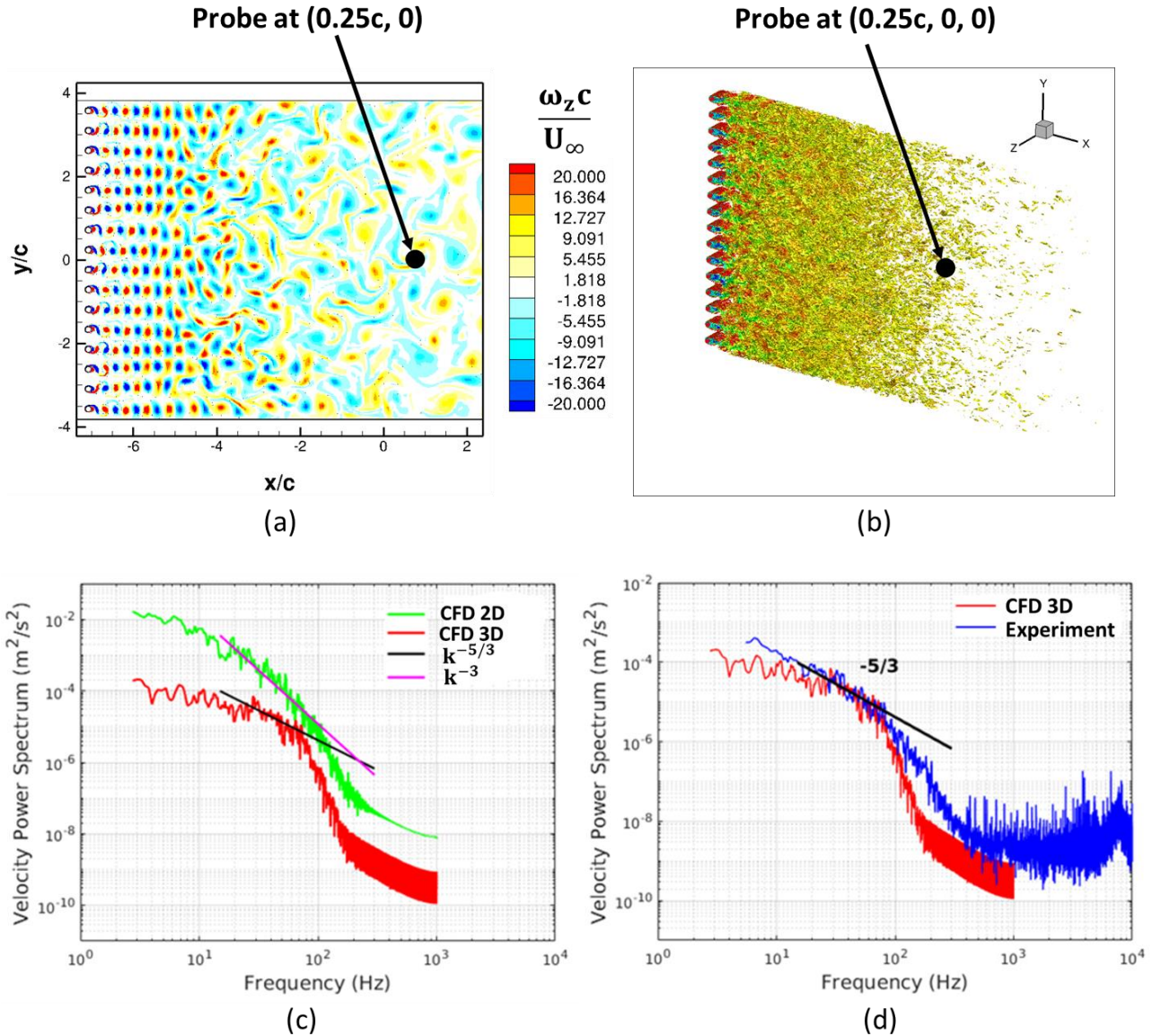


Figure 2: (a) 2D flow field in the downstream of an array of cylinders (b) 3D flow field in the downstream of an array of cylinders (c) Velocity Power Spectrum plot at the probe location for 2d and 3D results and (d) Velocity Power Spectrum plot at the probe location for 3D, and its comparison with the experimental results.

After confirming that the parallel array of cylinders produced similar turbulence to experimental measurements, a NACA0012 airfoil was placed in the computational domain at seven chord lengths away from the turbulence generator. This was done to match the experimental configuration in the ARL wind tunnel. At first a 2D simulation was conducted with varying angles of attack (α) to observe the impacts of this level of turbulence on the airfoil. While it is known that 2D simulations do not generate true turbulence at a wide range of scales, this simulation allowed for the investigation of multiple factors not possible in experimental studies. First, it is unknown whether large or small scale structures are the cause of the performance changes observed experimentally. By using the 2D simulation only larger scale and more coherent structures would be generated. Secondly, if the 2D simulation was successful at modeling the

aerodynamic performance it would allow for a fast method for calculating turbulence effects on airfoil performance. The vortices observed in the flow in the 2D simulations were, as expected, larger and the lack of breakdown into small structures was apparent, see Fig. 3. In this case it became apparent that the large-scale eddies were significantly impacting the airfoil and the 2D simulation was not likely to be successful at modeling turbulence effects.

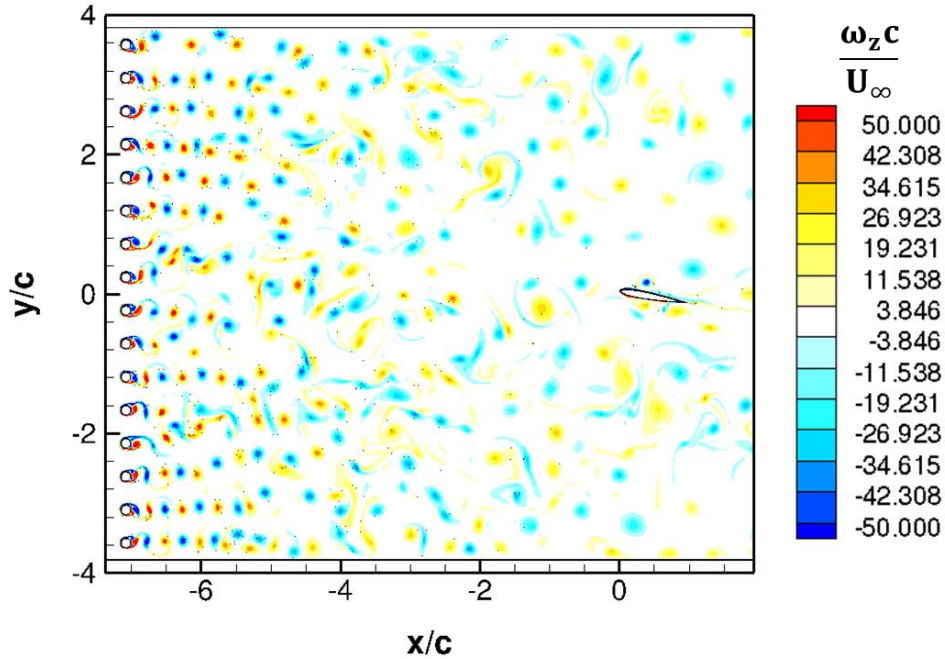


Figure 3: 2D Instantaneous Vorticity Field of a NACA0012 Airfoil at $\alpha = 10^\circ$ and $Re = 12,000$ with the Turbulence Generator.

Figure 4 shows a close-up flow field around the NACA0012 airfoil at $\alpha = 10^\circ$ with freestream turbulence present. The large vortex structures produced by the turbulence generator were observed randomly striking the airfoil, having a significant impact on the boundary layer and airfoil performance. Figures 4 (a-f) show the evolution of the flow over 30 non-dimensional times, during which many unsteady vortex-boundary layer interactions occurred. The formation of leading-edge vortices was random and dependent on the strength of the upstream vortices generated by the turbulence generator. This leading-edge vortex formation is somewhat similar to that observed on dynamic wings, but this effect is not observed in experimental studies, which had lower turbulence intensities.

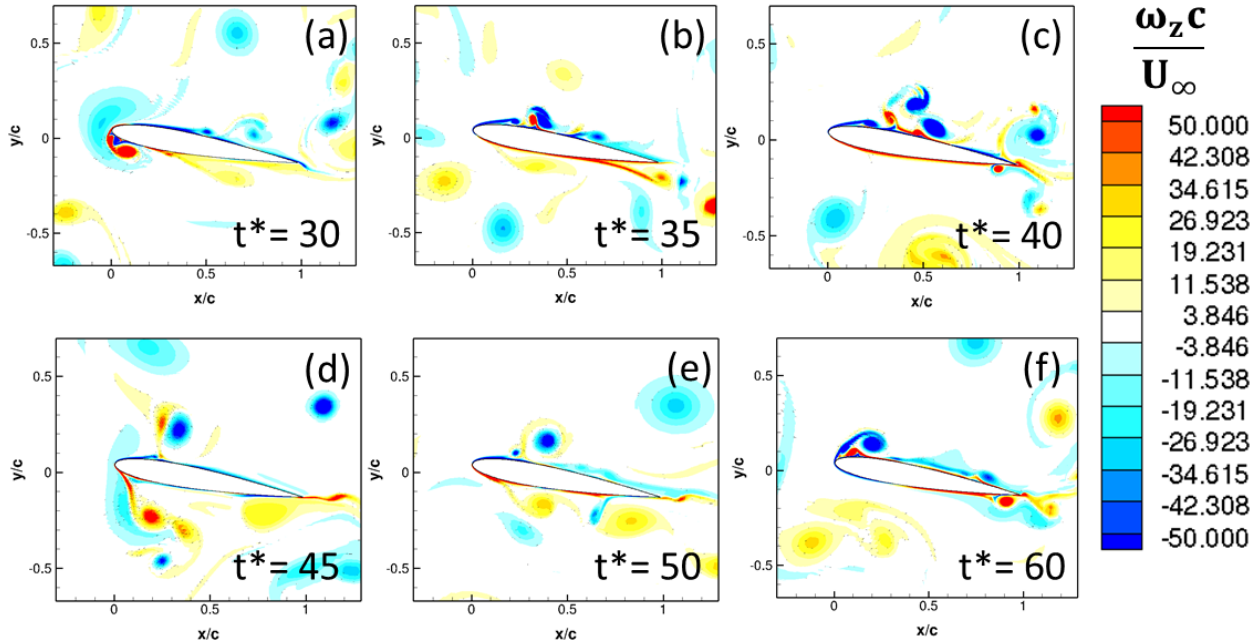


Figure 4: 2D Instantaneous Vorticity Fields on the NACA0012 at $\alpha = 10^\circ$ and $Re\ 12,000$ with the Turbulence Generator.

From the 2D simulation, the turbulence generator was not able to produce a uniform turbulence near the airfoil and boundary layer development was effectively random due to the strong vortex structures in the flow. These limitations of the 2D simulation suggested that a 3D simulation was needed to adequately model the airfoil performance. Partial 3D simulations, with a span of X and Y boundary conditions, produced a flow with nominally isotropic turbulence similar to that observed in experiment (see Figure 2). In order to study the impact of turbulence disturbance on the airfoil two cases were simulated with a 3D domain. A baseline NACA0012 in clean flow and with the Turbulence Generator (TG) were simulated to compare the effects of freestream turbulence on the stationary wing at the angle of attack $\alpha = 10^\circ$. The configuration of the TG was the same as for the 2D case, which is based off experiments at ARL and had a turbulence intensity of about 5%.

Figure 5 shows the flow field results of the 3D simulation for the airfoil at $\alpha = 10^\circ$, with Fig. 5(a) showing a 2D instantaneous vorticity and Fig. 5(b) showing 3-dimensional view of Q-Criterion. Results of the 3D simulation showed that vortices from the upstream turbulence generator were fundamentally different from those in the 2D simulations. The eddies in the region near the wing were generally more uniform in this case. The vortex stretching allowed by 3D simulations was shown to be necessary for the large vortices shed from the TG to break down into smaller scale turbulence. This effect more closely matched real-world turbulent breakdown as shown in Fig. 2(d).

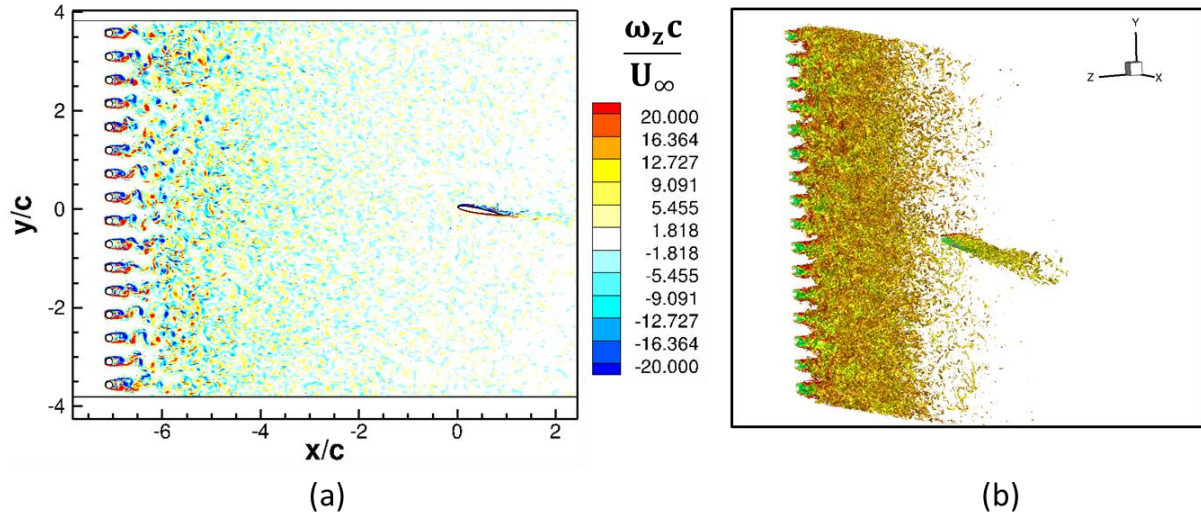


Figure 5: (a) A 2D view of the Instantaneous Vorticity Field and (b) the Iso-surface of Q colored by the streamwise velocity for the 3D simulation at $\alpha = 10^\circ$ and $Re=12,000$.

The boundary layer formation on the NACA0012 wing at $\alpha = 10^\circ$ due to the turbulence generator was significantly different compared to the baseline case. Figure 6 shows a close up view of the flow around the airfoil with and without freestream turbulence. In Figure 6 (a, c) a 2D instantaneous vorticity is shown with the corresponding iso-surface of the Q-criterion in Fig. 6(b, d). At $\alpha = 10^\circ$ on the baseline airfoil there was a clear flow separation and the airfoil was stalled. Conversely, for the same airfoil in turbulence the flow remained generally attached. The boundary layer was also notably different for the airfoil in turbulence when compared with the baseline. While the baseline airfoil at this angle was clearly stalled, the presence of turbulence reattached the flow and the airfoil was not in a stalled state. These results indicate that the stall angle of the airfoil was extended by turbulence, as previously reported by [14,16–18].

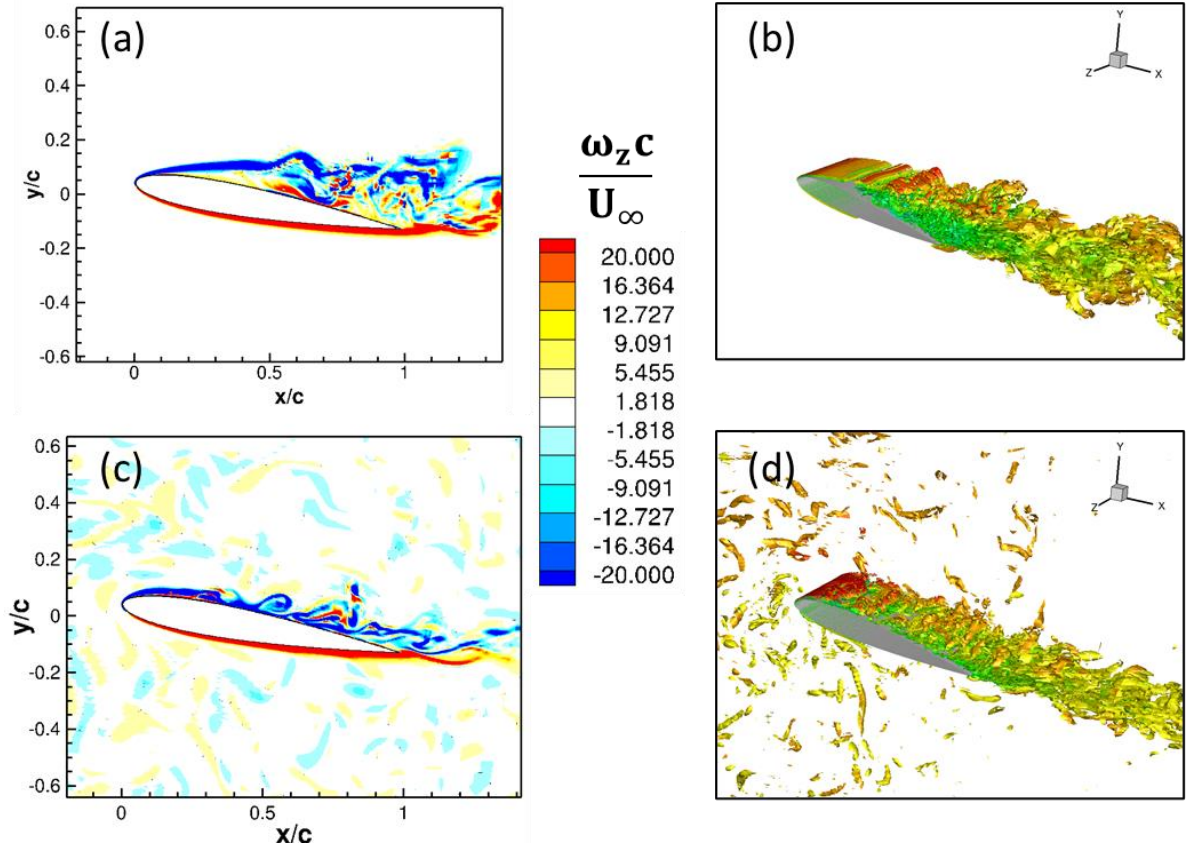


Figure 6: (a) A 2D view of $\alpha = 10^\circ$ wing with no TG, and (b) the corresponding iso-surface of Q colored by the streamwise velocity for 3D simulation at $\alpha = 10^\circ$ without TG. (c) A 2D view of $\alpha = 10^\circ$ wing with a MTG, and (d) the corresponding iso-surface of Q colored by the streamwise velocity for 3D simulation at $\alpha = 10^\circ$ with a MTG.

To further compare the effectiveness of 2D and 3D simulations for the modeling to airfoil performance in turbulence, a comparison of the lift performance was also done. Figure 7 shows the lift coefficient histories over the time for 2D and 3D simulations with turbulence present. In the 2D simulation large fluctuations in the force history was observed. The obvious reason for these large spikes in the lift in the 2D simulation was due to the interaction between large-scale vortices and the airfoil. However, because the 3D simulation allowed for large shed vortices to break down into small-scale eddies fluctuation of the lift was far less severe. These small scale vortices did however have a significant impact on the flow separation as seen in Fig. 6, which in turn had a large impact on the lift coefficient and stall angle. Interestingly, the time-averaged lift coefficients for the two cases were strikingly similar to each other, with the 2D simulation resulting in $C_L = 0.72$ and the 3D simulation resulting in $C_L = 0.77$. This result suggests that great care must be taken when modeling turbulent flows at low Reynolds numbers, as mean values may be similar but with strikingly different flow fields.

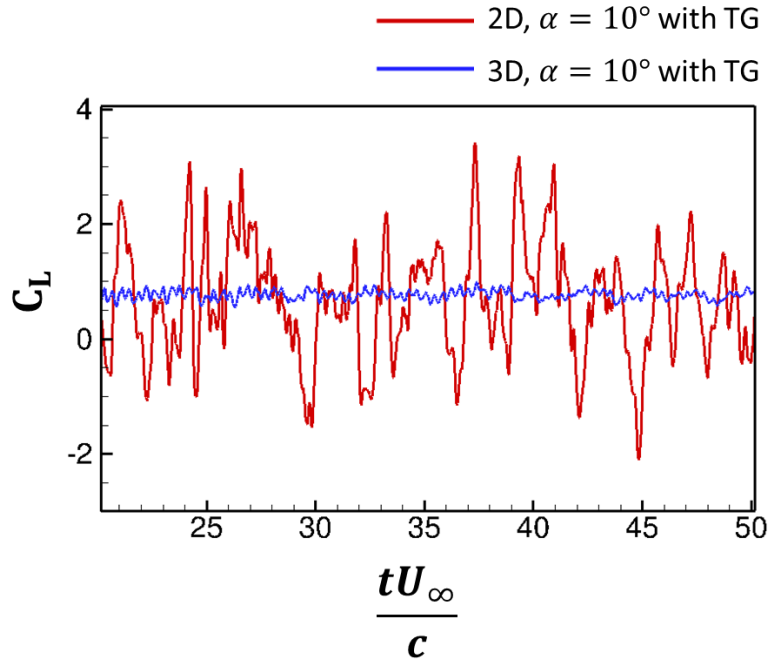


Figure 7: Lift coefficient histories for the 2D and 3D cases with the MTG for NACA0012 at $\alpha = 10^\circ$ and $Re = 12,000$.

Further analysis was done comparing the lift calculations at a wider range of angles of attack. Figure 8 shows the experimental and computational comparison of the time-averaged lift coefficients, as a function of angles of attack (α), for the baseline and turbulence generator cases. A preliminary 3D model using only 2nd order spatial and temporal schemes was evaluated and had poor performance modeling the lift of the baseline wing. It followed the baseline experimental data at low angles but deviated significantly at higher angles. Due to computational run time, a time-averaged lift coefficient for the 3D case for only $\alpha = 10^\circ$ with the 3rd order spatial and 4th order temporal schemes was conducted. These results agreed well with the experimental results with only a small discrepancy for the case with the MTG. It should be noted that the simulation agrees quite well with $\alpha = 9.5^\circ$ and $\alpha = 10.5^\circ$ and that experimental uncertainty at $\alpha = 10.0^\circ$ may explain this discrepancy. At $\alpha = 10^\circ$ the lift coefficient was higher when turbulence was present for both the simulation and experiment. The lift results from 2D simulations with the turbulence generator did not agree particularly well with the experimental results. However, these results may superficially appear to be accurate if care isn't taken to compare to comparable experiments. More investigations are needed to answer the question to what extent 2D simulations could reliably predict airfoil performance in unsteady freestream flows.

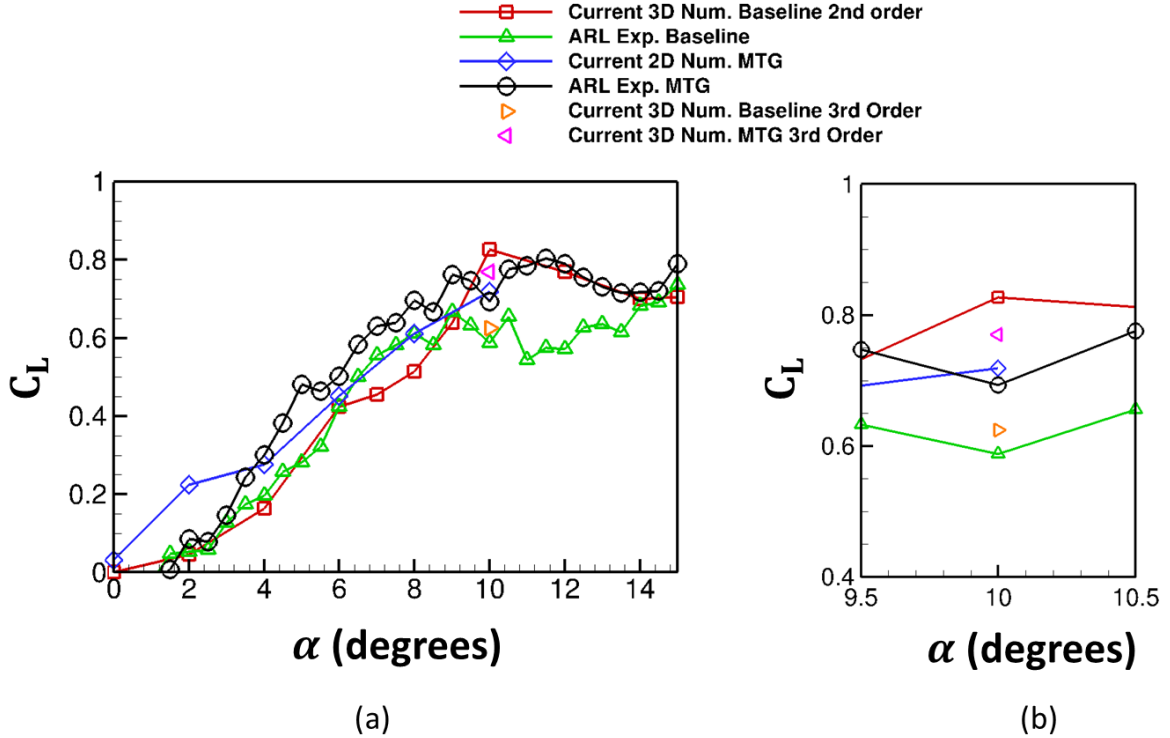


Figure 8: (a) The Time-averaged lift coefficients as a function of α for $Re=12,000$ and (b) Close view of average lift coefficient around 10 degrees.

V. Conclusion and Future Work

Freestream turbulence was shown again to have a significant influence on the aerodynamic performance of a NACA0012 airfoil at the low Reynolds number, 12,000. A turbulence generation mechanism was developed that adequately reproduced grid turbulence when compared with wind tunnel experiments. The turbulence generated in 3D simulations were shown to closely match turbulence statistics from wind tunnel experiments. Separate 2D simulations were ineffective at reproducing experimental turbulence due to lack of vortex stretching. This resulted in slower vortex breakdown and larger scale vortices in the flow. The large-scale vortices dominated airfoil performance, producing a larger force fluctuation on the airfoil, but with similar average lift as higher fidelity simulations. The 3D simulations allowed for faster turbulent breakdown of large scale structures in the flow, more closely resembling real-world turbulence. The small-scale structures did not generate large force fluctuation, but did significantly alter boundary layer evolution. The background turbulence from the turbulence generator caused the flow to remain attached on the suction side of the airfoil at $\alpha = 10^\circ$, while this same airfoil in a uniform freestream is stalled. Due to this the lift coefficient was also higher with turbulence compared to the uniform freestream case. More work must be done to study the impact of the turbulence generators with varying turbulence intensity levels and at a wider angles of attack range. This work has shown that any further computational modeling of static airfoil performance at low Reynolds number with freestream turbulence requires a high-order method with 3D simulations to obtain accurate results.

Acknowledgements

This research was supported in part by an appointment to the Science Education and Workforce Development Programs at Oak Ridge National Laboratory, administered by ORISE through the U.S. Department of Energy Oak Ridge Institute for Science and Education. Research was partially supported by the Combat Capabilities Development Command - Army Research Laboratory under CRADA 14-054-003. The views and conclusions in this document are those of the authors and should not be interpreted as representing the official policies, either expressed or implied, of the Army Research Laboratory or the U.S. Government. The U.S. Government is authorized to reproduce and distribute reprints for Government purposes notwithstanding any copyright notation herein. The hardware used in the computational studies is part of the UMBC High Performance Computing Facility (HPCF). The facility is supported by the U.S. National Science Foundation through the MRI program (grant nos. CNS-0821258, CNS-1228778, and OAC-1726023) and the SCREMS program (grant no. DMS-0821311), with additional substantial support from the University of Maryland, Baltimore County (UMBC).

References

- [1] Jones, G., Santer, M., Debiasi, M., and Papadakis, G. "Control of Flow Separation around an Airfoil at Low Reynolds Numbers Using Periodic Surface Morphing." *Journal of Fluids and Structures*, Vol. 76, 2018, pp. 536–557. <https://doi.org/10.1016/j.jfluidstructs.2017.11.008>.
- [2] Watkins, S., Milbank, J., Loxton, B. J., and Melbourne, W. H. "Atmospheric Winds and Their Implications for Microair Vehicles." *AIAA Journal*, Vol. 44, No. 11, 2006, pp. 2591–2600. <https://doi.org/10.2514/1.22670>.
- [3] Cleaver, D. J., Wang, Z., and Gursul, I. "Investigation of High-Lift Mechanisms for a Flat-Plate Airfoil Undergoing Small-Amplitude Plunging Oscillations." *AIAA Journal*, Vol. 51, No. 4, 2013, pp. 968–980. <https://doi.org/10.2514/1.J052213>.
- [4] Chen, J. M., and Choa, C.-C. "Freestream Disturbance Effects on an Airfoil Pitching at Constant Rate." *Journal of Aircraft*, Vol. 36, No. 3, 1999, pp. 507–514. <https://doi.org/10.2514/2.2485>.
- [5] McGhee, R. J., Walker, B. S., and Millard, B. F. *Experimental Results for the Eppler 387 Airfoil at Low Reynolds Numbers in the Langley Low-Turbulence Pressure Tunnel*. National Aeronautics and Space Administration, 1988, p. 234.
- [6] Zhou, Y., and Wang, Z. Effect of Surface Roughness on Laminar Separation Bubble over a Wing at a Low-Reynolds Number. Presented at the 49th AIAA Aerospace Sciences Meeting including the New Horizons Forum and Aerospace Exposition, Orlando, Florida, 2011.
- [7] Hoffmann, J. A. "Effects of Freestream Turbulence on the Performance Characteristics of an Airfoil." *AIAA Journal*, Vol. 29, No. 9, 1991, pp. 1353–1354. <https://doi.org/10.2514/3.10745>.
- [8] Laitone, E. V. "Wind Tunnel Tests of Wings at Reynolds Numbers below 70 000." *Experiments in Fluids*, Vol. 23, No. 5, 1997, pp. 405–409. <https://doi.org/10.1007/s003480050128>.
- [9] Mish, P. F., and Devenport, W. J. Mean Loading Effects on the Surface Pressure Fluctuations on an Airfoil in Turbulence. Maastricht, Netherlands, 2001.
- [10] Gilling, L., Sørensen, N., and Davidson, L. Detached Eddy Simulations of an Airfoil in Turbulent Inflow. 2009.
- [11] Huang, R. F., and Lee, H. W. "Effects of Freestream Turbulence on Wing-Surface Flow and Aerodynamic Performance." *Journal of Aircraft*, Vol. 36, No. 6, 1999, pp. 965–972. <https://doi.org/10.2514/2.2537>.

- [12] Wang, S., Zhou, Y., Alam, Md. M., and Yang, H. “Turbulent Intensity and Reynolds Number Effects on an Airfoil at Low Reynolds Numbers.” *Physics of Fluids*, Vol. 26, No. 11, 2014, p. 115107. <https://doi.org/10.1063/1.4901969>.
- [13] Conger, R. N., and Ramaprian, B. R. “Pressure Measurements on a Pitching Airfoil in a Water Channel.” *AIAA Journal*, Vol. 32, No. 1, 1994, pp. 108–115. <https://doi.org/10.2514/3.11957>.
- [14] Cruz, E. G. *The Effect of Turbulence on Micro Air Vehicle Airfoils*. PhD Dissertation. RMIT University, Melbourne, Australia, 2012.
- [15] Sicot, C., Aubrun, S., Loyer, S., and Devinant, P. “Unsteady Characteristics of the Static Stall of an Airfoil Subjected to Freestream Turbulence Level up to 16%.” *Experiments in Fluids*, Vol. 41, No. 4, 2006, pp. 641–648. <https://doi.org/10.1007/s00348-006-0187-9>.
- [16] Delnero, J., Marañón Di Leo, J., Bacchi, F., Colman, J., and Boldes, U. “Experimental Determination of the Influence of Turbulent Scale on the Lift and Drag Coefficients of Low Reynolds Number Airfoils.” *Latin American applied research*, Vol. 35, No. 3, 2005, pp. 183–188.
- [17] Tsuchiya, T., Numata, D., Suwa, T., and Asai, K. Influence of Turbulence Intensity on Aerodynamic Characteristics of an NACA 0012 at Low Reynolds Numbers.
- [18] Ravi, S., Watkins, S., Watmuff, J., Massey, K., Marino, M., and Petersen, P. Influence of Turbulence Intensity on the Flow Structure over a Thin Airfoil at Lower Reynolds Numbers. Presented at the ICAS 2012, Australia, 2012.
- [19] Coder, J. G., and Maughmer, M. D. “Comparisons of Theoretical Methods for Predicting Airfoil Aerodynamic Characteristics.” *Journal of Aircraft*, Vol. 51, No. 1, 2014, pp. 183–191. <https://doi.org/10.2514/1.C032232>.
- [20] Yu, M., and Wang, L. “A High-Order Flux Reconstruction/Correction Procedure via Reconstruction Formulation for Unsteady Incompressible Flow on Unstructured Moving Grids.” *Computers & Fluids*, Vol. 139, 2016, pp. 161–173. <https://doi.org/10.1016/j.compfluid.2016.05.028>.
- [21] Wang, Z. J., and Gao, H. “A Unifying Lifting Collocation Penalty Formulation Including the Discontinuous Galerkin, Spectral Volume/Difference Methods for Conservation Laws on Mixed Grids.” *Journal of Computational Physics*, Vol. 228, No. 21, 2009, pp. 8161–8186. <https://doi.org/10.1016/j.jcp.2009.07.036>.
- [22] Huynh, H. T. A Flux Reconstruction Approach to High-Order Schemes Including Discontinuous Galerkin Methods.
- [23] Vincent, P. E., Castonguay, P., and Jameson, A. “A New Class of High-Order Energy Stable Flux Reconstruction Schemes.” *Journal of Scientific Computing*, Vol. 47, No. 1, 2011, pp. 50–72. <https://doi.org/10.1007/s10915-010-9420-z>.
- [24] Wang, L., and Yu, M. On the Parallel Implementation and Performance Study of High-Order Rosenbrock-Type Implicit Runge-Kutta Methods for the FR/CPR Solutions of the Navier-Stokes Equations.
- [25] Wang, L., and Yu, M. “Comparison of ROW, ESDIRK, and BDF2 for Unsteady Flows with the High-Order Flux Reconstruction Formulation.” *Journal of Scientific Computing*, Vol. 83, No. 2, 2020, p. 39. <https://doi.org/10.1007/s10915-020-01222-z>.
- [26] Wang, L., and Yu, M. Jacobian-Free Implicit p-Adaptive High-Order Compact Direct Flux Reconstruction Methods for Unsteady Flow Simulation.
- [27] Roe, P. L. “Approximate Riemann Solvers, Parameter Vectors, and Difference Schemes.” *Journal of Computational Physics*, Vol. 43, No. 2, 1981, pp. 357–372. [https://doi.org/10.1016/0021-9991\(81\)90128-5](https://doi.org/10.1016/0021-9991(81)90128-5).
- [28] Bassi, F., and Rebay, S. “A High-Order Accurate Discontinuous Finite Element Method for the Numerical Solution of the Compressible Navier–Stokes Equations.” *Journal of Computational Physics*, Vol. 131, No. 2, 1997, pp. 267–279. <https://doi.org/10.1006/jcph.1996.5572>.
- [29] Abrahamsen Prsic, M., Ong, M. C., Pettersen, B., and Myrhaug, D. “Large Eddy Simulations of Flow around a Smooth Circular Cylinder in a Uniform Current in the Subcritical Flow Regime.” *Ocean Engineering*, Vol. 77, 2014, pp. 61–73. <https://doi.org/10.1016/j.oceaneng.2013.10.018>.